

# Application of Onboard PIV to Front Wheelhouse Wake Behavior under Stationary Crosswind Conditions

N. Kuratani<sup>1\*</sup>

1: Innovation Research Excellence, Honda R&D Co., Ltd, Japan

\* Correspondent author: Naoshi\_Kuratani@jp.honda

**Keywords:** Onboard PIV, Front Wheelhouse Wake, Crosswind, POD and DMD

## ABSTRACT

When driving a car, the driver and passengers may feel larger drag from a headwind, the steering wheel would be taken away by a crosswind or pushed by a tailwind. Anytime, anywhere, we will encounter various scenes with natural wind under real world conditions such as urban, suburb and highway. We will develop the appropriate vehicle by simulating these conditions to satisfy with various customer requirements. For vehicle aerodynamic research and development, we are simply running simulations in physical- and cyber-space, that is, wind tunnel facility and computational fluid dynamics to reproduce these real worlds. However, it is not easy to simulate these wind inlet conditions, such as the temporal change in crosswind, especially, in wind tunnel facility. The stationary yaw angle by rotating turntable would reproduce a crosswind, if there is no turbulent generator system like in Pininfarina and Swing in FKFS. Therefore, we focus on the unsteady and asymmetrical flow from the front wheelhouse of the vehicle with tire rotation. There is three-dimensional complicated flow that are interacted by the flow from various directions, such as the flow along the front bumper, the flow along the rotating tire and wheel, the blowing flow from the rotating wheel opening area and the flow from the tire house. These complicated flow produces the front wheelhouse wake along the body side that affects the vehicle aerodynamic performance. Furthermore, there are asymmetrical flows around the vehicle by different front wheelhouse wake in windward and leeward sides. The larger side wake increases the aerodynamic drag, and the fluctuating side wake may induce the instability of the vehicle handling stability. Here, the proposed onboard 2D-3C PIV measurement system in the previous study enables us to measure same measurement area along the vehicle body side without change in optical configuration effectively, that indicates to reduce the time by resetting the optical configuration. We will investigate what kind of flow field should be focused on and controlled to prevent the vehicle instability by investigating these asymmetrical flow field around the vehicle under crosswinds.

---

## 1. Introduction

"How beautiful the Earth can we leave for future generations?" This is a major challenge today to achieve sustainable society all over the world. These rapid changes in the global environment are forcing the automotive industry to undergo a once-in-a-century transformation. There are various options for achieving the carbon neutrality, and manufacturers and suppliers are making tireless efforts every day to achieve these technological innovations. As alternative fuels to gasoline, there are fuel technologies such as hydrogen and ammonia, electrification with zero CO<sub>2</sub> emissions, and hybrid technologies that combine them, but each has its advantages and disadvantages.

However, regardless of what type of power unit is used to achieve the carbon neutrality, the importance of aerodynamic technology that contributes to reducing drag and improving handling stability will not change significantly. When it comes to electrification, until the energy density of onboard batteries improves or infrastructure such as quick chargers is developed, vehicles with long driving ranges will be chosen, so there is a strong demand for the evolution of more low-drag aerodynamic performance. Cooling is essential for any power unit, and it is essential to achieve both low drag and cooling performance. Furthermore, the lower the drag of the vehicle body, the more robustness against disturbances such as road surface input or natural wind is required, and the greater the demand for understanding and technology of unsteady flow phenomena than for low drag and stable handling stability. Therefore, we believe that measurement technology that can measure unsteady flow phenomena around real scale vehicle is essential to advance aerodynamic technology in real-world conditions. In this study, we investigated in detail the changes in the flow around the real scale vehicle under conditions simulating a crosswind in a certain direction using the measurement technology proposed in a previous study.

Most of the previous studies on the unsteady flow field around rotating tires have been performed using computational fluid dynamics, CFD (Elofsson 2002, Takeuchi 2016, Hurlbrink 2019, Ambo 2017, Ambo 2020, Nagaoka 2024), and there have been few experimental studies of body side wake under steady yaw angle conditions (Waschle 2007, Haff 2017). The purpose of this study is to clarify the different front wheelhouse wake patterns between the windward and leeward sides under stationary yaw angle conditions with aerodynamic configurations by this onboard time-series 2D-3C PIV measurement (Kuratani 2022). We will investigate what kind of flow field should be focused on and controlled to keep low drag aerodynamic performance and to prevent the vehicle instability by investigating these asymmetrical flow field around the vehicle under crosswinds.

## **2. Experimental apparatus and conditions**

### **2.1. Wind tunnel with single moving ground belt**

The wind tunnel experiments were performed in the wind tunnel (Koremoto 2010, Koremoto 2011) owned by Honda R&D Co., Ltd. This wind tunnel has open jet type and a  $6.7 \times 3.6$  [m<sup>2</sup>] 3/4 nozzle, and this test section is 14.5 [m] length. The fan in this wind tunnel has maximum power of 3.6 [MW] and produces 1,400 [m<sup>3</sup>/s] with 8 [m] diameter and 24 rotor vanes made with carbon fiber-reinforced plastic and 35 stator vanes with steel. The feature of this wind tunnel facility is a single moving belt system to simulate the running conditions. This single belt has 3.2 [m] width and 9 [m] length, which is distance between front and rear rollers, and only 1 [mm] thickness of stainless-steel belt. And this single moving belt can be operated up to 300 [km/h]. And a boundary layer

removal system has primary scoop for removing the developed boundary layers at the exit of nozzle and secondary suction and tangential blowing at upstream of the single belt. Aerodynamic force measurement system has combined horizontal force and wheel force measurement systems. The former one can measure the drag and side force at the structural members of single moving belt system, the latter one can measure lift force by load cells installed under stainless steel belt with air bearing system, respectively. Test vehicle is always fixed by four hub bearings, but in this study, only one hub and rod are removed to investigate the flow field on single moving belt. The 12.3 [m] diameter turntable can be rotated from +10deg. to -10deg. in synchronization with single belt rolling road system to simulate stationary crosswind conditions.

## 2.2. Test road vehicle and configurations

The 10<sup>th</sup> Generation *CIVIC* (Honda Motors Co. Ltd.) as compact sedan (*Length*=4,650 [mm], *Width*=1,800 [mm], *Height*=1,415 [mm]) was used for wind tunnel test in this study as shown in Figure 1. However, in this study only one hub bearing and rod at front side was removed not to disturb the flow around rotating tire and wheel as shown in Figure 1 in detail. The (b) Grille Close indicates that the incoming flow into engine room for cooling system will be shut down, that causes to reduce the aerodynamic drag and to produce the minus front lift force due to this flow coming into the underfloor to increase the mass flow rate as shown in Figure 2. The front strake is in front of front tire and is used for aerodynamic drag reduction. The (c) Front Strake Off indicates removing this Front Strake. And (d) Wheel Cover On indicates that there is no flow through the wheel opening area with tire and wheel rotation. These four configurations including (a) Baseline are compared to investigate the wake patterns around rotating front tire and wheel under stationary yaw angle conditions.

And the change in stationary yaw angle is rotated by turntable as shown in Figure 3. This onboard PIV system installed on the right side of the vehicle, clockwise rotation means plus yaw angle and counterclockwise rotation means minus one. So, the plus yaw angle shows leeward side and minus yaw angle does windward, as shown in Figure 3.

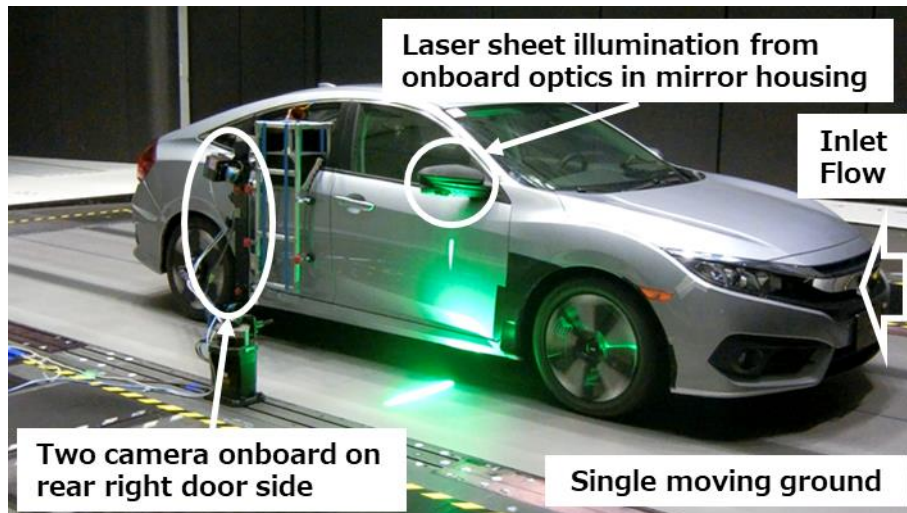


Fig. 1 Overview of wind tunnel testing under running with onboard PIV measurement system.

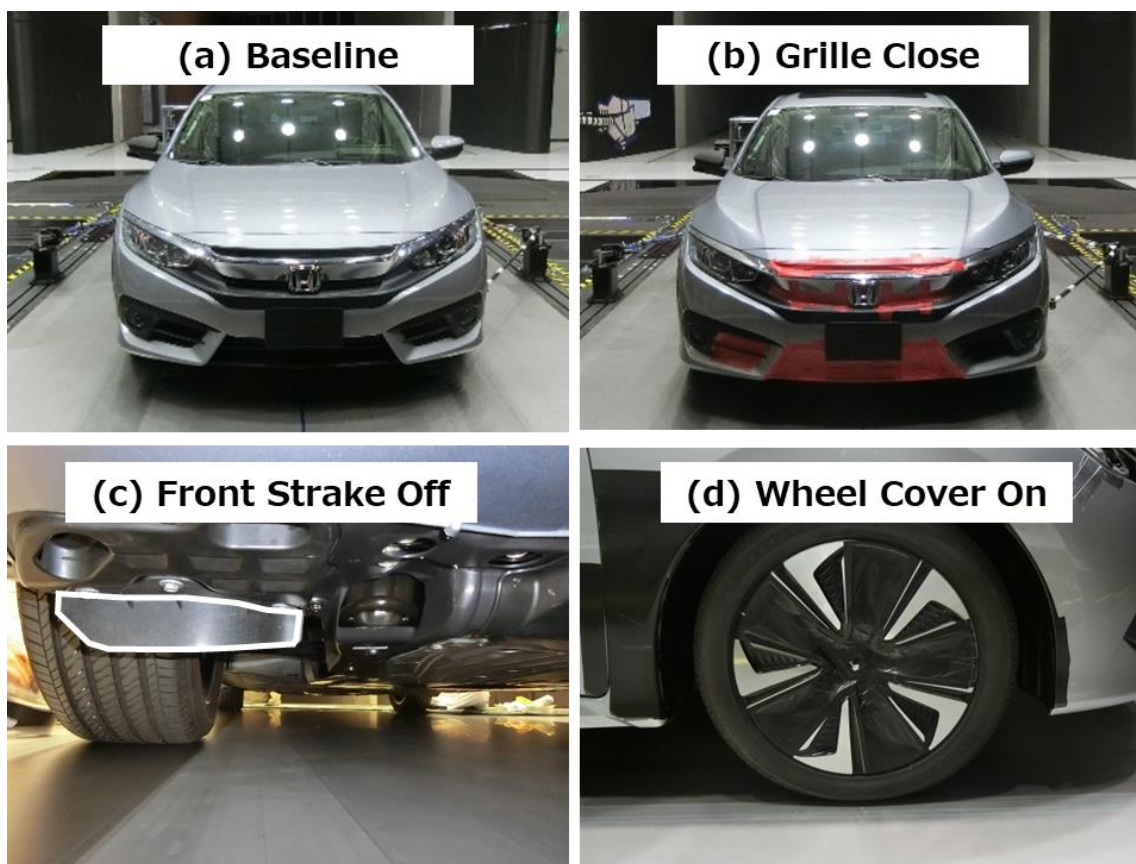
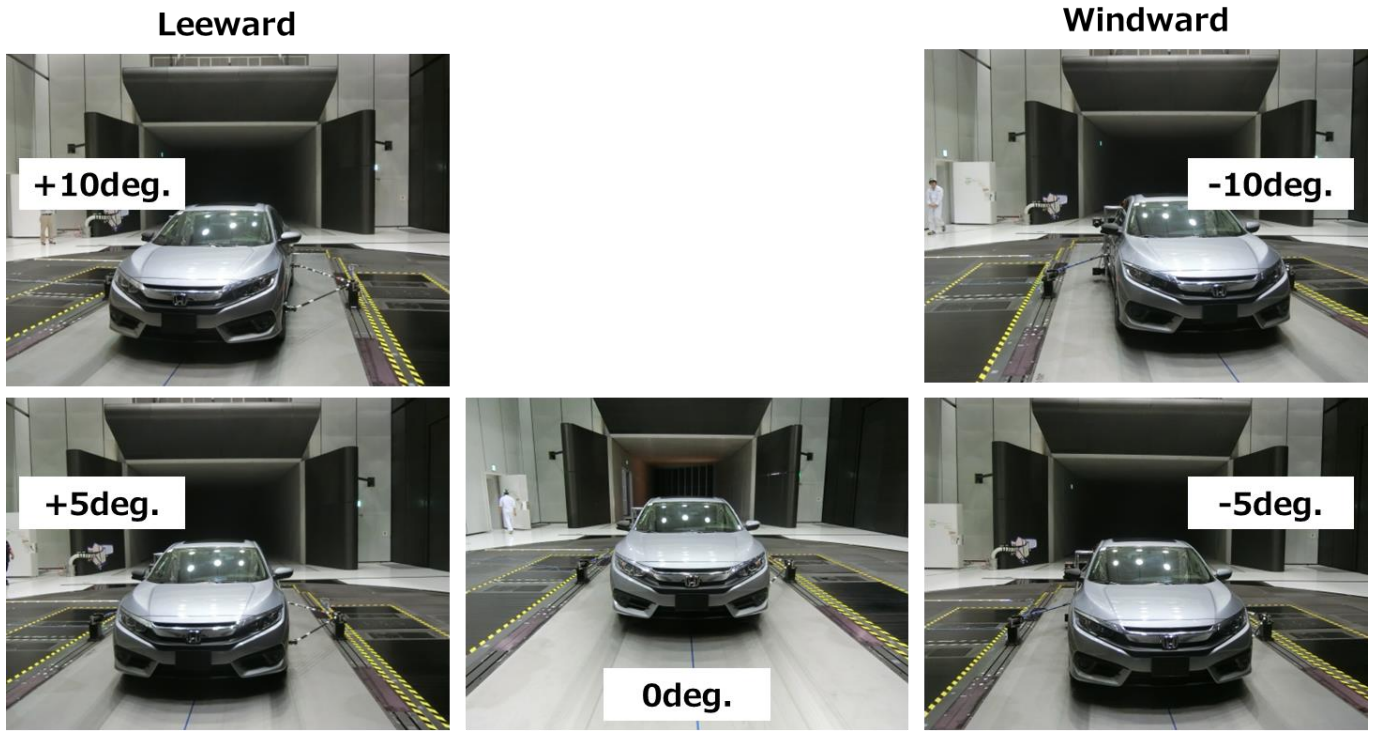


Fig. 2 Aerodynamic configurations of test vehicle with (a) Baseline, (b) Grille Close, (c) Front Strake Off and (d) Wheel Cover On.



**Fig. 3** Front view of test vehicle under stationary yaw angle conditions from -10 deg. windward to +10deg. leeward by rotating turntable.

### 2.3. Onboard high-speed 2D-3C PIV measurement system

PIV measurement as known as non-intrusive flow measurement is usually performed to measure the flow around the object by external optical access such as laser sheet, however, this laser sheet illumination causes the stronger laser light reflection on the surface of object. And the treating mat black aluminum on the surface of object, the pasting the anti-reflective sheet on the surface of subject or reducing the laser power is selected to avoid the strong laser light reflection, respectively. This laser light reflection makes the deterioration of signal to noise ratio of the particle image. Therefore, in this study, onboard PIV measurement system as shown in Figure.4 was proposed to avoid the stronger laser light reflection. These components of this onboard PIV are installed inside of the test vehicle as shown in Figure.4. Laser source, laser and camera synchronized controller (LC880, LabSmith) and control PC (DELL Precision T3610) are equipped inside of test vehicle and power supply and chiller of laser source are equipped in the trunk of test vehicle. This laser source is a high-repetition pulsed laser (18 [W], 1 [kHz], 527 [nm], DM20, Photonics Industries). These two high speed cameras (1024 x 1024 [pixels], miniAX200, Photoron) with Nikon  $f = 85$  [mm] lens (AF-S NIKKOR 85mm f/1.4, Nikon Corporation) were installed on the right and rear side door of test vehicle to capture the y-z plane from downstream of measurement plane. Laser light sheet optics with optical fiber to transfer laser are installed in right side mirror to illuminate the laser sheet around rotating front tire and wheel. As results, this optical configuration enables us to avoid the stronger laser light reflection on the exterior body surface. PIV Measurement area is 300 [mm] width and 300 [mm] around rotating front tire and wheel as shown in Figure.4. This center point

of measurement area is located at 150 [mm] horizontally from the surface of front door side panel and at 550 [mm] height from the ground due to keeping the pinch angle = 30 [degree] between two cameras. The wind tunnel test conditions are shown in Table 1. The running speed was set to 100 [km/h] as free stream velocity. To simulate the stationary crosswind conditions, the plus 5 and 10 yaw angle shows leeward side and minus 5 and 10 yaw angle does windward in Table 1. A large amount of uniform oil mist of about 3 [μm] can be generated by seeding generator including 4 nozzles (CTS-4000, SEIKA Digital Image Corporation). DOS is used for seeding oil and these oil mist can follow the flow and reduce the contamination of wind tunnel and test vehicles. These oil mist were provided at collector and circulated in this wind tunnel.

**Table 1** Test vehicle aerodynamic configurations and test conditions.

Case	Aerodynamic Configuration	Vinf [km/h]	Yaw Angle [deg.]
(a)	Baseline	100	-10 (Windward)
(b)	Grille Close		-5
(c)	Front Strake Off		0 (Straight)
(d)	Wheel Cover On		+10 (leeward)

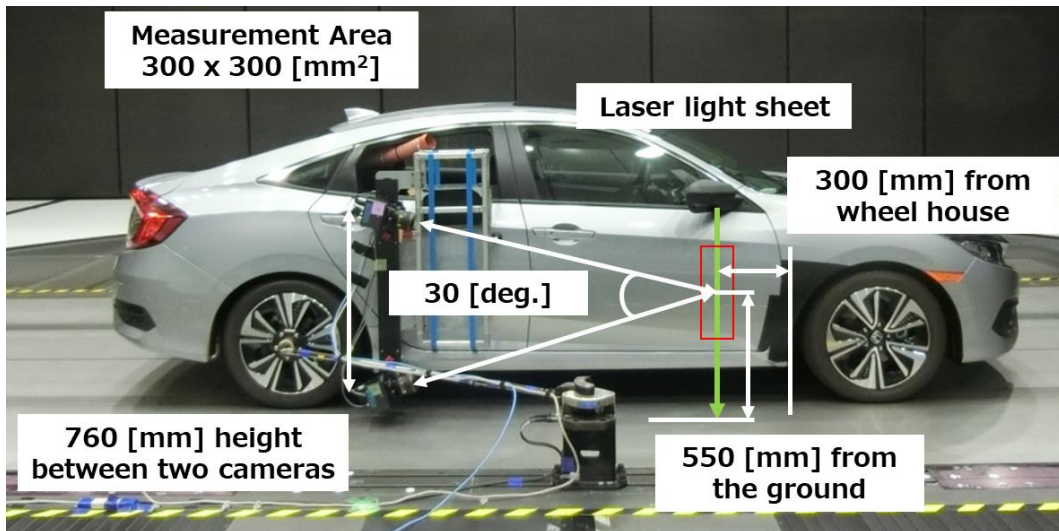


**Fig. 4** Schematics of the onboard 2D-3C PIV measurement system on the right side of vehicle.

Laser illumination pulse width is 40 [μsec] at frequency 800 [Hz]. Interrogation window size was 32 x 32 [pixels] with 50% overlap, the spacing between vectors was in  $y$ -direction and  $z$ -direction was 5.40 [mm] as a result. Each 2700 shots of time series particle images were measured at 800 [Hz] during about 3.5 [seconds]. These image data were stored in about 15 [minutes] and only 100 paring data were analyzed for quick review in 10 [minutes]. Koncerto II (SEIKA Digital Image Corporation) was used for measurement control and analyzing the velocity field. After that, the data analysis as post processing is operated by MATLAB to execute POD and DMD analysis.

### 3. Results and discussions

#### 3.1. Windward and leeward side wake under stationary yaw angle conditions

At first, this onboard PIV measurement proposed in the previous study (Kuratani 2022) was performed under stationary yaw angle conditions as shown in Table 1 from -10 deg. windward to +10deg. leeward by rotating turntable. Figure 5 show the time-averaged velocity magnitude flow field. From the top to bottom, there are aerodynamic configurations, (a) Baseline, (b) Grille Close, (c) Front Strake Off and (d) Wheel Cover On. From the left, the windward side, yaw angle = -10, -5deg., and to the right, leeward side, yaw angle = +5 or +10 deg. In case of (a) Baseline, there are strongly different wake between windward and leeward sides. The windward side, yaw angle = -5 or -10 deg., shows the air flow comes to the right-side body directly and there is the flow along the body side, therefore, this flow is not separated. On the other hand, the leeward side, yaw angle = +5 or +10 deg., shows the larger flow separation from the right-side body due to the large flow separation from the front hood, front bumper or fender. In case of (b) Grill Close, we can see the different wake patterns between (a) Baseline and (b) Grill Close at yaw angle = +5deg. Grill Close means the incoming flow is decreased due to the front cooling opening closed as shown in Figure 2. This effect shows the smaller wake at Yaw=0deg. and +5deg. to compare with (a) Baseline and (b) Grill Close. However, yaw angle = +10 deg., there is larger wake development in case of (b) Grill Close. Because large stationary yaw angle produces the larger flow separation from the front hood, front bumper or fender. These remarkable results show, in case of (b) Grill Close, the non-symmetrical flow at smaller yaw angle, but asymmetrical flow at larger yaw angle.

Let us show the different aerodynamic configuration, (c) Front Strake Off and (d) Wheel Cover On. It is easy to understand the remarkable wake development in case of (c) Front Strake Off than the other cases due to the higher-pressure field in front tire house without Front Strake in front of front tire, as shown in Figure 2, under all stationary yaw angle conditions. And in case of (d) Wheel Cover On, there are smaller wake than that of (a) Baseline under each yaw angle conditions due to suppressing the blowing flow from the wheel opening area with tire and wheel rotation. However, that of (d) Wheel Cover On is larger than (b) Grill Close, because (b) Grill Close shut down the incoming flow into the engine room and suppresses the flow into the front tire house. These time-averaged velocity magnitude flow field clarified the remarkable phenomena around the front wheelhouse wake under the stationary yaw angle conditions.

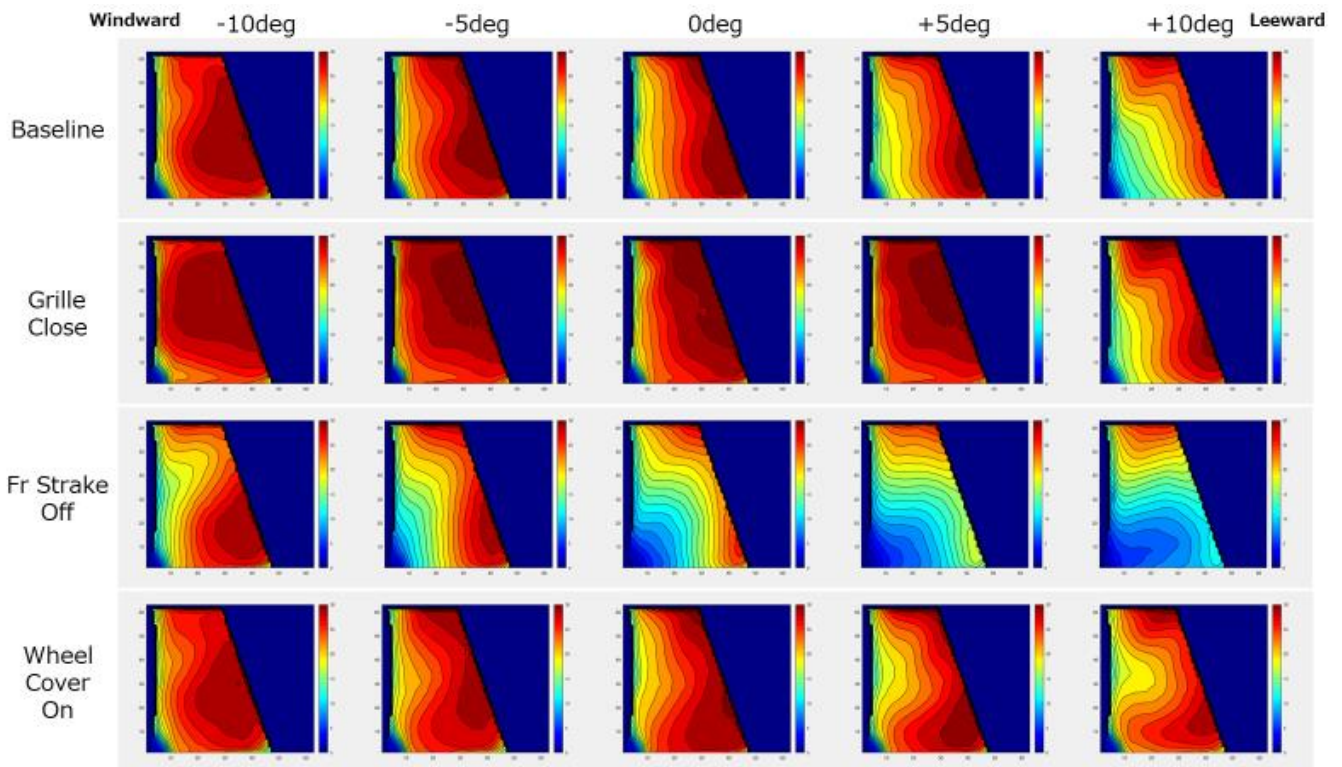


**Fig. 5** Time averaged velocity magnitude flow field under stationary Yaw angle, -10 to +10 deg, (a) Baseline, (b) Grill Close (c) Front Strake Off and (d) Wheel Cover On

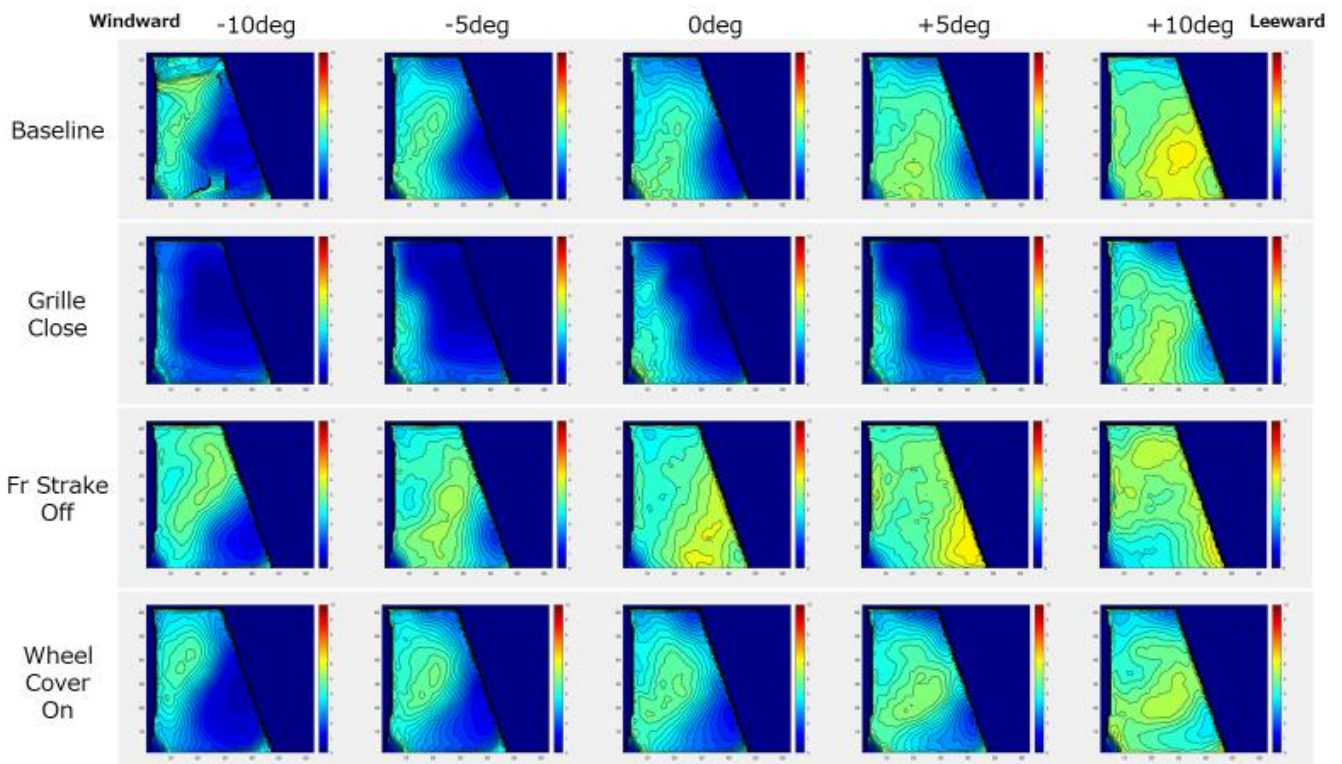


**Fig. 6** Fluctuating velocity magnitude flow field under stationary Yaw angle, -10 to +10 deg, (a) Baseline, (b) Grill Close (c) Front Strake Off and (d) Wheel Cover On

### 3.2. Fluctuating Flow Field in Windward and leeward side wake under stationary yaw angle conditions

Figure 6 show the standard deviation of velocity magnitude, that is, velocity fluctuation in the measurement area same as shown in Figure 5 under same aerodynamic configurations and yaw angle conditions.

There is remarkable fluctuation by aerodynamic configurations and stationary yaw angle conditions. At first, there is smaller fluctuation in mainstream to compare with Figure 5 and 6, for example, in case of (a) Baseline, at yaw angle= 0deg. There is higher velocity field with lower flow fluctuation, which is mainstream. There is lager wake development at yaw angle= +10deg. in case of (a) Baseline, there is larger flow fluctuation in the wake. In case of (c) Front Strake Off, there is larger fluctuation under the stationary yaw angle conditions due to the higher-pressure field in front tire house. Although (b) Grill Close and (d) Wheel Cover On show similar time averaged flow fields as shown in Figure 5, the areas of fluctuation are different as shown in Figure 6. In case of (b) Grill Close at yaw angle= +10deg on the leeward side, there is the wake from a wide range in the height direction, that is, from the front tire house and wheel opening area. And in case of (d) Wheel Cover On, there is the wake from the gap between the front tire house and front tire, that is, blowing flow.

To focus on the asymmetrical flow at windward and leeward sides, the time averaged and fluctuation flow field are compared with yaw angle= +5/-5deg in case of (a) Baseline and (b) Grill Close. In case of (a) Baseline, there is asymmetrical flow at these angles, on the other hand, in case of (b) Grill Close, there is symmetrical flow due to the less outflow from front tire house and wheel openings area. As results, these fluctuation area of (b) Grill Close are considerably smaller that of (a) Baseline. This result suggests the possibility of suppressing fluctuation to the vehicle body side.

We can easily identify the development and fluctuation locations of these front wheelhouse wakes to compare with time averaged and fluctuating velocity fields, respectively. There is a great advantage that we can investigate the asymmetrical flow field between windward and leeward sides more clearly with this onboard PIV measurement system.

### 3.3. Time averaged and Fluctuating Flow Field of Lateral Velocity in Windward and leeward side wake under stationary yaw angle conditions

Figures 7 and 8 show the time-averaged lateral velocity flow field and the standard deviation of lateral velocity, respectively, same as shown in Figures 5 and 6 under same aerodynamic configurations and yaw angle conditions. In case of (a) Baseline and yaw angle = +10 deg, leeward

side, there are larger lateral velocity field in the upper that indicates the strongly wake from the front tire house., therefore, different wake between windward and leeward sides.

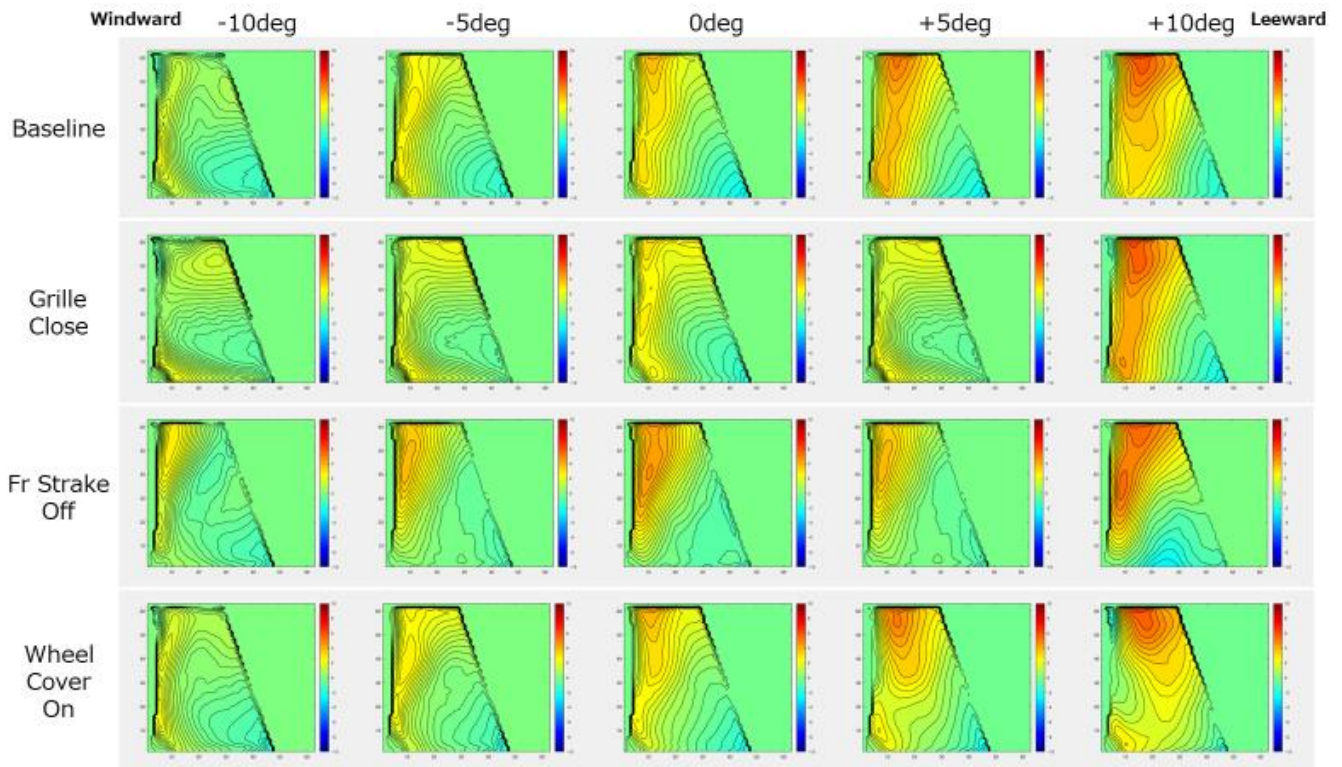


**Fig. 7** Time averaged lateral velocity flow field under stationary Yaw angle, -10 to +10 deg, (a) Baseline, (b) Grill Close (c) Front Strake Off and (d) Wheel Cover On

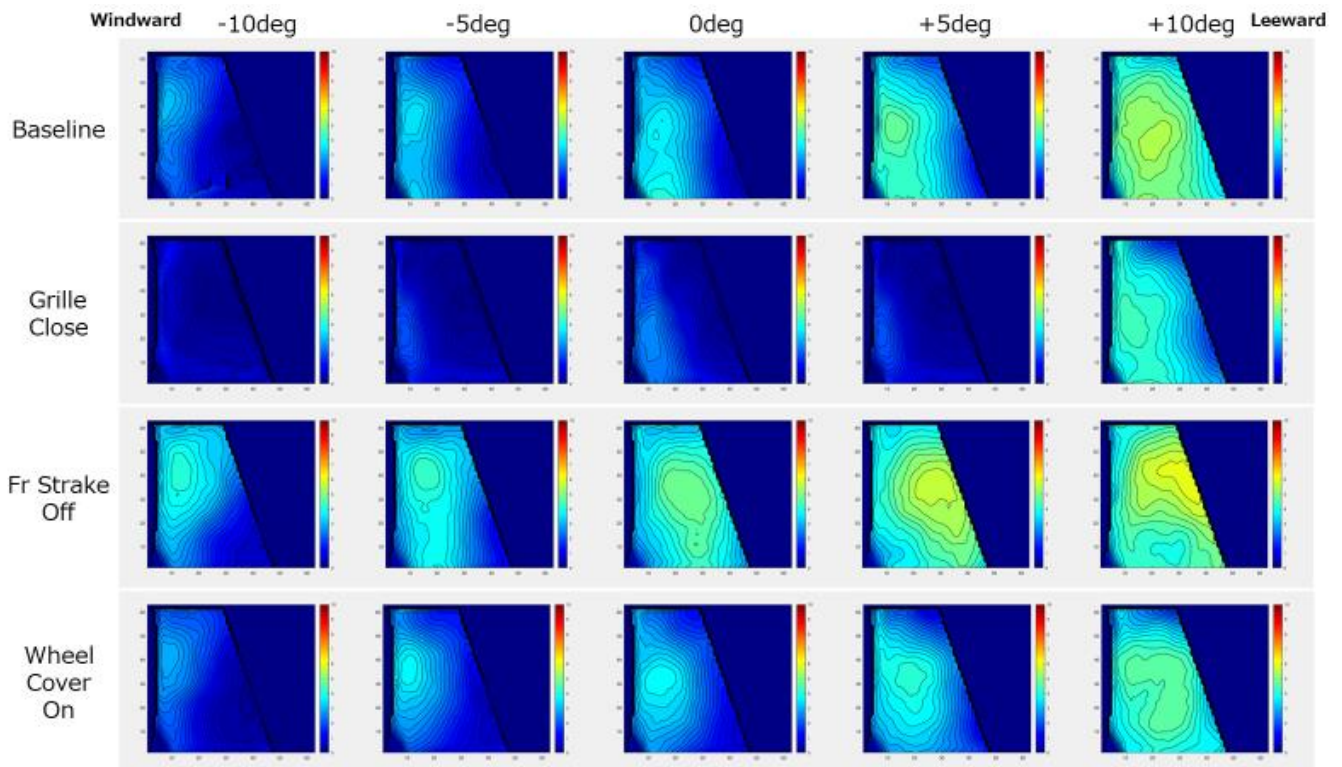


**Fig. 8** Fluctuating y-component velocity flow field under stationary Yaw angle, -10 to +10 deg, (a) Baseline, (b) Grill Close (c) Front Strake Off and (d) Wheel Cover On

The windward side, yaw angle = -5 or -10 deg., shows the air flow comes to the right-side body directly and there is the flow along the body side, therefore, this flow is not separated. On the other hand, the leeward side, yaw angle = +5 or +10 deg., shows difference in the flow on the leeward sides clearly. In case of (a) Baseline and (d) Wheel Cover On, there is lateral flow at +5deg., while in (b) Grill Close it develops at larger +10deg. In these cases of (a) Baseline and (d) Wheel Cover On, fluctuating lateral flow gradually becomes stronger as the yaw angle increases in leeward sides. But, in case of (b) Grill Close, there is weaker fluctuating flow at smaller +5deg. And, in case of (c) Front Strake Off, this lateral velocity is a little weaker at smaller +5deg than straight at 0deg, but it becomes stronger at larger +10deg. This change is non-linearity. This result along the vehicle body side suggests the possibility of inducing instability in vehicle dynamics under real world with natural wind conditions. We can easily identify these locations where asymmetry occurs from these changes in time averaged and fluctuating lateral flow field as shown Figures 7 and 8.

### 3.4. Extracting wake modes by DMD analysis

It is difficult to say that the essential flow features can be extracted just by calculating the statistics from tremendous measurement data. Therefore, in this study, Dynamic Mode Decomposition, DMD, is applied to extract the spatiotemporal flow features and has been used in various data analyses. We will not go into the details of the DMD analysis here due to space limitations. For more information, please refer to this reference (Kutz 2017). At first, DMD analysis was applied to the velocity magnitude flow fields in case of (a) Baseline and (c) Front Strake Off, as shown in Figures 9 and 10. These figures show the time-averaged flow field and DMD mode #1 to #7 of velocity magnitude under stationary yaw angle, from -10 to +10 deg. DMD mode #1 show the time-averaged one, so we must focus on the modes from #2. As the number of DMD modes increases, the DMD mode pattern becomes smaller, which is the same as in Proper Orthogonal Decomposition, POD, analysis (Kuratani 2022). Comparing the differences in yaw angle with the same DMD mode #2, the condition where the pattern size is the largest matches the condition where the larger wake at +10deg. on the leeward side. Under leeward side at yaw angle, +10 deg., comparing (a) Baseline and (c) Front Strake Off, the mode patterns are different, but the pattern size is similar due to the wake development in leeward side. Comparing windward and leeward sides in the same DMD mode #2 in case of (a) Baseline and (c) Front Strake Off, these different mode patterns indicate the asymmetrical flow around the vehicle. Furthermore, unlike POD, DMD analysis provides not only the modes but also a set of associated eigenvalues that determine a low dimensional dynamical system for how the mode amplitudes evolve in time. These time dynamics will be performed to extract the characteristic spatiotemporal information of front wheelhouse wake by DMD analysis.

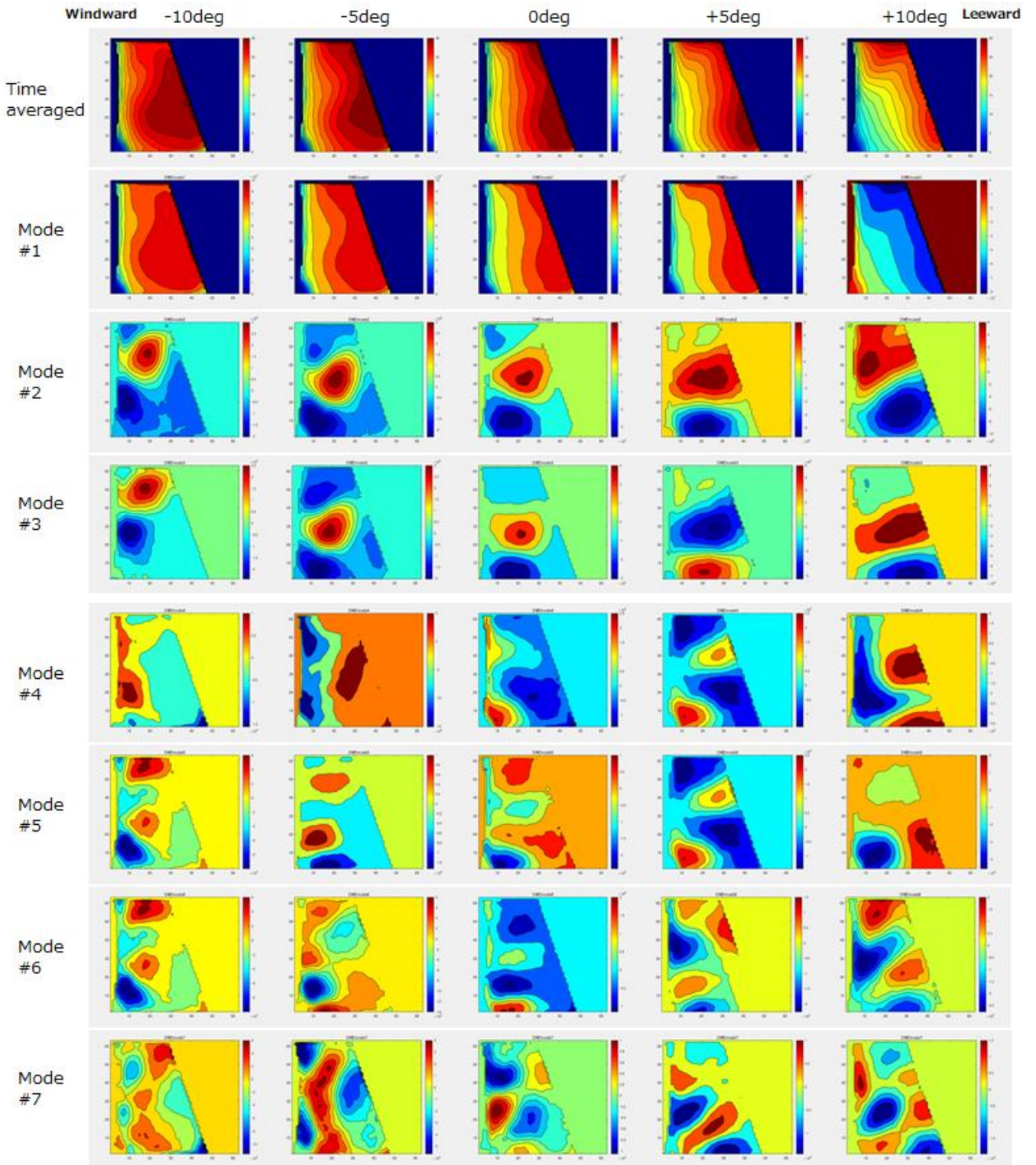


Fig. 9 Application of DMD analysis on velocity magnitude field from mode #1 to #7 with time averaged flow field in case of (a) Baseline under stationary Yaw angle, -10 to +10 deg.

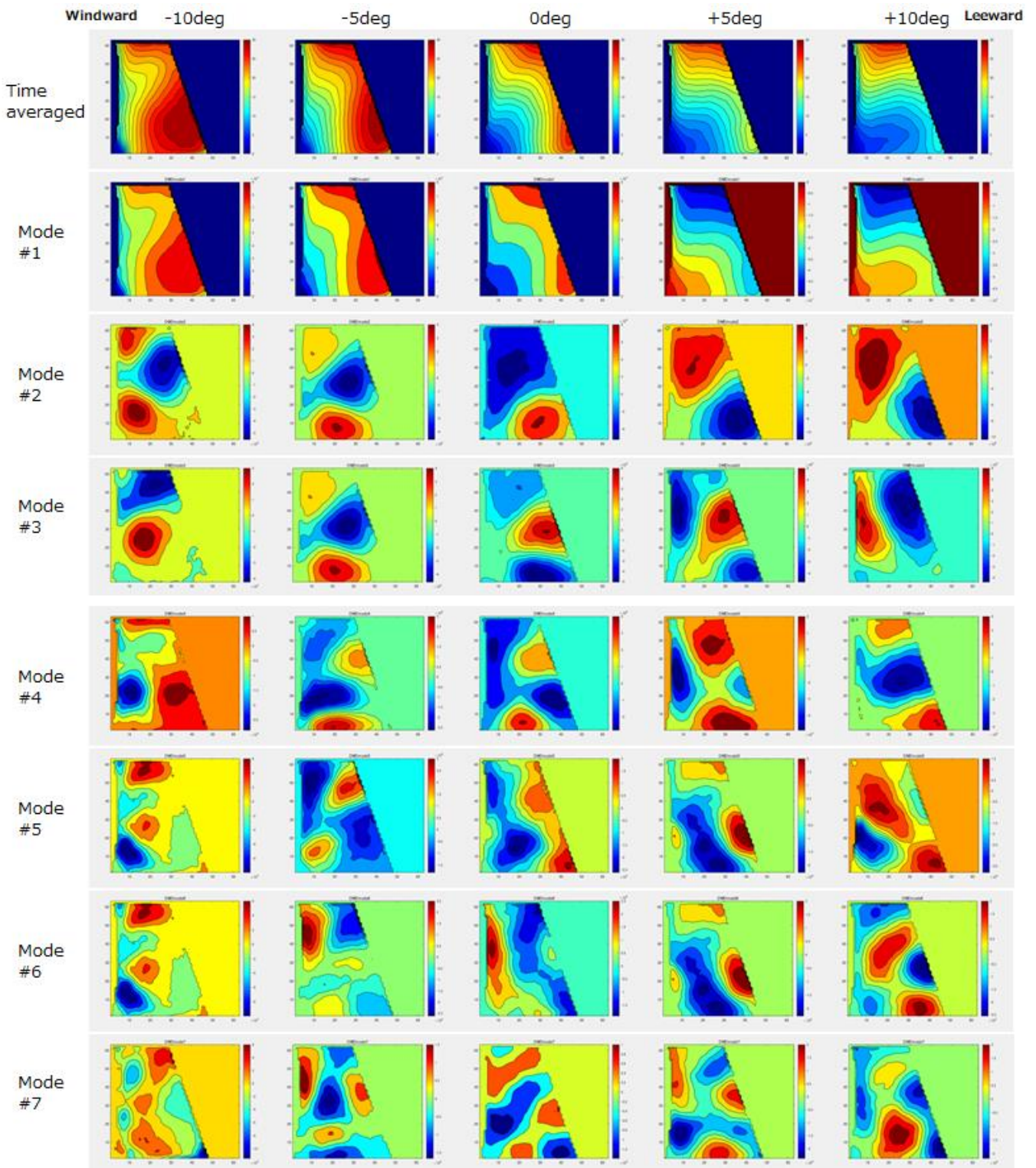


Fig. 10 Application of DMD analysis on velocity magnitude field from mode #1 to #7 with time averaged flow field in case of (c) Front Strake Off under stationary Yaw angle, -10 to +10 deg.

POD analysis can perform the mode decomposition by arranging the flow field in order of increasing energy, but there is a problem in that temporal characteristics are lost. DMD analysis was performed in order to extract the spatiotemporal characteristics of the flow field. First, the cumulative value of the modes excluding the mean field is calculated, and the number of modes when the proportion of the total energy is set to 70% is obtained. FFT analysis of the absolute

velocity magnitude was performed on the data set reconstructed up to that mode, and the frequency distribution was shown as Figure 11. The power spectrum density obtained from the frequency analysis at each measurement point was not averaged for each frequency, but the 97.5% quantile of the power spectrum density at each frequency was calculated.

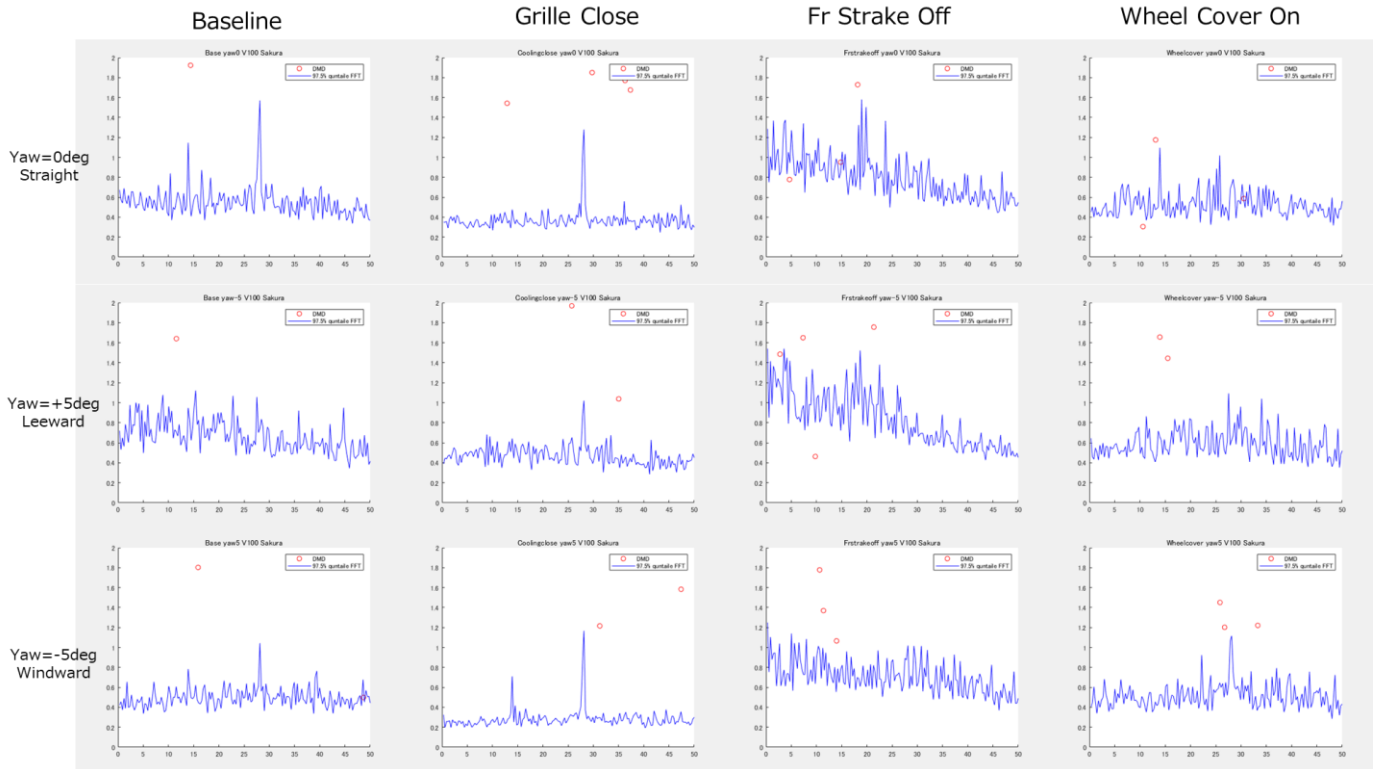


Fig. 11 Application of FFT and DMD analysis on velocity magnitude field in case of (a) Baseline, (b) Grill Close (c) Front Strake Off and (d) Wheel Cover On, under stationary Yaw angle = 0, +5 (Leeward) and -5 (Windward) deg.

As a result in case of Yaw=0deg., there are two clear peak frequency as shown in (a) Baseline. They depend on the tire rotation and show harmonics due to the presence or absence of the wheel opening. This can also be seen from the fact that the harmonics did not appear when the wheel opening was closed in (d) Wheel Cover On. On the other hand, there is no first peak frequency due to the smaller wheel house wake in (b) Grill Close and power spectrum density is smaller than that of (a) Baseline. This result indicates that the vehicle handling instability is better under high-speed driving. In case of (c) Front Strake Off, there is the largest power spectrum density than the others. This is the worst case under high-speed driving due to the stronger power spectrum density around the vehicle's natural frequency around 1-2Hz lower than the first peak frequency related with tire rotation.

There is larger wake development under leeward condition than windward as shown in stronger power spectrum density. In case of (b) Grill Close, there is clear first peak frequency due to the tire

rotation, because more the air flows into the front wheel-house under wind ward condition, however, power spectrum density is lower in low frequency range. These figures show the left-right asymmetry caused by these stationary crosswind conditions, it is believed that reducing flow fluctuation using these aerodynamic devices would be effective in further controlling vehicle stability under high-speed driving.

#### 4. Conclusions and Future works

This innovative on-board 2D-3C PIV measurement system in wind tunnel facility with moving ground has been developed to measure the same measurement area along the vehicle body side without change in optical configuration effectively, that indicates to reduce the time by resetting the optical configuration under the stationary yaw angle conditions.

These averaged velocity field enable us to understand the effect of aerodynamic devices under straight condition, under  $\text{Yaw}=0\text{deg}$ . In particular, the Grill Close, Front Strake and Wheel Cover affect the smaller front wheel-house wake that enables the lower drag performance and flow fluctuation around the vehicle. Under stationary windward and leeward conditions, there is asymmetry flow field around the vehicle body. Furthermore, these aerodynamic devices affect the lower power spectrum density of velocity magnitude to enable us to keep the vehicle stability under high-speed driving.

Even under stationary yaw angle conditions, we were able to discuss the asymmetry flow field around the vehicle body under real-world natural wind conditions. However, in order to realize real-world measurements, several improvements are strongly required, such as making the measurement system smaller, lighter, and easier to operate, as well as seeding particles to prevent contamination of facilities.

#### 7. References

- Per Elofsson, Mark Bannister (2002) Drag Reduction Mechanism Due to Moving Ground and Wheel Rotation in Passenger Cars. SAE Technical Paper 2002-01-0531
- Alexander Waschle (2007) The Influence of Rotating Wheels on Vehicle Aerodynamics – Numerical and Experimental Investigations. SAE Technical Paper 2007-01-0107
- Kensuke Koremoto, Nobuyuki Kawamura, Naoshi Kuratani, Shinsuke Nakamura, Toshihiro Arai (2010) The Characteristics of the Honda Full Scale Aero-acoustic Wind Tunnel equipped with a Rolling Road System. 8th MIRA International Vehicle Aerodynamic Conference

- Kensuke Koremoto, Nobuyuki Kawamura, Michihiro Aoki, Naoshi Kuratani, Shinsuke Nakamura, Hideki Yoshioka (2011) Full-scale Wind Tunnel Equipped with Single-belt Rolling Road System. Article of Honda R&D Technical Review Vol.23 No.1
- Kanade Takeuchi, Tetsuhiro Kawamura, Naoshi Kuratani, Akira Kobayakawa, Yasuo Osawa, Makoto Tsubokura (2016) LES on the aerodynamic effect of tire shapes with moving ground using a detailed full-scale vehicle model. International Conference on Vehicle Aerodynamics 2016
- Kei Ambo, Takashi Yoshino, Tetsuhiro Kawamura, Minoru Teramura, David A. Philips, Guillaume A. Bres, Sanjeeb T. Bose (2017) Comparison between Wall-modeled and Wall-resolved Large Eddy Simulations for the prediction of boundary-layer separation around the side mirror of a full-scale vehicle. AIAA Paper 2017-1661
- Johannes Haff, Sven Lange, Henning Wilhelmi (2017) An Experimental Study of the Under-Floor Flow of a VW Golf 7 under On-Road and Wind-Tunnel Conditions via Particle Image Velocimetry. 11<sup>th</sup> FKFS conference: Progress in Vehicle Aerodynamics and Thermal Management
- Kunihiro Taira, Brunton, S. L., Dawson, S., Rowley, C. W., Colonius, T., McKeon, B. J., Schmidt, O. T., Gordeyev, S., Theofilis, V., and Ukeiley, L. S. (2017) Modal Analysis of Fluid Flows: An Overview. AIAA Journal, Vol. 55, No. 12, 2017, pp. 4013–4041.
- Jelena Hurlbrink, Tarik Barth, Christoph Lietmeyer, Alexander Wittmaier, Jörg Seume (2019) Analysis of the Flow Topology and Loss Mechanisms in the Wheelhouse Area. 12<sup>th</sup> FKFS conference: Progress in Vehicle Aerodynamics and Thermal Management
- Kei Ambo, Hiroaki Nagaoka, D. Philips, C. Ivey, G. Brès, S. Bose (2020) Aerodynamic force prediction of the laminar to turbulent flow transition around the front bumper of the vehicle using Dynamic-slip wall model LES. AIAA Paper 2020-0036
- Naoshi Kuratani, Tetsuhiro Kawamura, Kei Ambo (2022) Wake Patterns Around Front Tyre And Wheel On Vehicle Dynamics Clarified By On-Board PIV Application. PROCEEDINGS OF THE 20th International Symposium on the Application of Laser and Imaging Techniques to Fluid Mechanics
- J. Nathan Kutz, Steven L. Brunton, Bingni W. Brunton, Joshua L. Proctor (2017) Dynamic Mode Decomposition: Data-Driven Modeling of Complex Systems, Society for Industrial and Applied Mathematics
- Hiroaki Nagaoka, Basim Yenerdag, Kei Ambo, David Philips, Christopher Ivey, Guillaume Brès, and Sanjeeb Bose (2024) Prediction of Aerodynamic Drag in SUVs with Different Specifications by Using Large-Eddy Simulations, SAE Technical Paper 2024-01-2525, 2024, doi:10.4271/2024-01-2525.